Journal of Materials Chemistry A

PAPER

View Article Online
View Journal | View Issue

Cite this: J. Mater. Chem. A, 2019, 7, 1300

High throughput identification of Li ion diffusion pathways in typical solid state electrolytes and electrode materials by BV-Ewald method†

Dajun Chen,[a] Jianshu Jie,[a] Mouyi Weng,[a] Shucheng Li,[a] Dong Chen,[a] Feng Pan *[a] and Lin-Wang Wang*[b]

Viewing the possible Li-ion migration pathways in solid state electrolytes and electrode materials is an important prerequisite for the development of all-solid-state battery materials. For high throughput material screening, it is important to have fast methods to determine the possible Li-ion pathways. In this study, by combining the traditional bond valence (BV) method with the Ewald summation method, a new BV-Ewald method was developed to calculate the Li ion diffusion map. The advantage of the new method is the improvement on the traditional BV method by taking into account the cation–cation Coulomb repulsion. By adjusting the isosurface value, the BV-Ewald method can effectively reveal the Li pathways of several well-studied electrolytes (*e.g.* Li_3OCl, $LiTi_2(PO_4)_3$, α-Li_3N and β-Li_3N) and cathode materials (*e.g.* $LiFePO_4$, $LiMn_2O_4$) and match with the experimental and *ab initio* calculation results. Furthermore, this new high throughput method was used for the fast prediction of Li-ion 1D, 2D and 3D-pathways of (anti)perovskite, NASICON, LISICON, garnet, Li-nitride, Li-hydride, Li-halide and argyrodite types of crystals with 34 different known electrodes and electrolytes as representatives. Hence, the new BV-Ewald method will help in the fast discovery of potential solid electrolyte materials.

Received 27th September 2018
Accepted 6th December 2018

DOI: 10.1039/c8ta09345h

rsc.li/materials-a

1. Introduction

Lithium (ion) batteries (LIBs) have been widely used in devices such as mobile phones, notebook computers[1] and hybrid electric vehicles[2,3] due to their large specific capacity, long storage and cycle life, and environmental friendliness. However, current LIBs mainly use liquid electrolytes that can easily leak and cause safety problems.[4] All-solid-state batteries consisting of solid electrodes and solid electrolytes[5] are promising next-generation LIBs. One of the primary conditions for both inorganic solid electrodes and solid electrolytes is high lithium ionic conductivity and connected lithium ion pathways. Experimentally, lithium ion channels can be measured directly by neutron diffraction.[6,7] Theoretically, Li ion migration pathways can be acquired by the first-principles simulations.[8–11] These can be direct *ab initio* molecular dynamics (MD) simulations or barrier height nudge elastic band (NEB) calculations. However, such calculations can be very expensive (the MD simulation) or require prior knowledge for the transition paths (NEB). Because of these difficulties, such *ab initio* methods are not suitable for high throughput screening of possible solid electrolyte or electrode materials. Some computationally fast methods could be extremely useful for either high throughput screening or to provide initial insights for more in-depth *ab initio* studies (*e.g.* using NEB). There are several methods for such purpose. One is the bond valence (BV) method,[10–14] while the others are geometry-based methods such as Voronoi–Dirichlet partition (VDP),[15] colony surface,[16] and procrystal analysis.[17] The geometry-based methods rely solely on the crystal structure and bonding topology and do not take into account any actual potential energies. The BV model has been widely used in crystallography to determine the positions occupied by atoms in the crystal structure[18] as well to visualize Li pathways.[12,17] However, when BV is used to visualize the Li pathway, it only takes into account the effects of the surrounding anode atoms, and ignores the electrostatic repulsion of the cations.[18] This can lead to some erroneous results, *e.g.*, the Li concentration on top of other cation atoms. It is this aspect of the BV method we aimed to improve in the current study.

We combined the BV theory and the Ewald summation, which is used to calculate the Coulomb repulsive force between Li ions and other cations, to improve the original BV method. Only the Coulomb interactions with cation atoms were included since the interactions with anion atoms have already been described by the BV model. We performed calculations for several materials and compared the results with *ab initio* molecular dynamics simulations and found that they are in

[a]School of Advanced Materials, Peking University, Shenzhen Graduate School, Shenzhen 518055, People's Republic of China. E-mail: panfeng@pkusz.edu.cn
[b]Materials Science Division, Lawrence Berkeley National Laboratory, Berkeley, California 94720, USA. E-mail: lwwang@lbl.gov

† Electronic supplementary information (ESI) available. See DOI: 10.1039/c8ta09345h

good agreement. By further analyzing the results, we found that the new BV-Ewald method was an improvement over the original BV method for many structures, such as Li_3N and $LiFePO_4$. In $LiFePO_4$, the original BV model yields Li density on top of the Fe atom, a clearly unphysical result. In Li_3N the BV model yields different Li diffusion paths compared with the *ab initio* results. Both these errors have been corrected by the BV-Ewald method. Finally, we calculated the Li pathways of 34 typical cathode/anode electrodes and solid electrolyte materials and determined the dimensionalities of their transition paths, *i.e.*, whether it is 1D, 2D or 3D path. We can obtain not only the Li diffusion pathways, but also other ionic diffusion pathways such as those for Na in sodium ion batteries. There are already many studies on the screening of sodium-based layered materials for sodium ion batteries.[19–21] Our method can also be used in this area to further screen sodium ion battery materials.

2. Methodology

The original BV method was put forward by Ian David Brown to describe the relationship between bond length and charge transfer: the shorter the bond length, the larger the charge transfer between the cation and anions.[18] It includes four heuristic principles: principle of maximum symmetry, electroneutrality principle, principle of local charge neutrality and equal valence principle.[18] The valence charge transfer based on the cation–anion bond length is described by

$$S_{\mathrm{A-X}} = \exp\left[\frac{R_0 - R_{\mathrm{A-X}}}{b}\right] \tag{1}$$

Then, the valence charge on atom A is described as

$$V(\mathrm{A}) = \sum_{\mathrm{X}} S_{\mathrm{A-X}} \tag{2}$$

In the above equations, A is the cation and X is the anion, $R_{\mathrm{A-X}}$ is their distance. R_0 and b are empirical parameters. $S_{\mathrm{A-X}}$ is the bond valence of A contributed by X in the given position and V(A) is the BV sum that should be close to the ideal chemical valence V_{ideal}(A). Thus, the deviation between V(A) and V_{ideal}(A) determines the energy of this structure. BV theory does not require a specific distinction between covalent and ionic types of bonding. Cations and anions are defined by their electronegativity and are equivalent to Lewis acids and bases.[19] In practice, we can assume that the central cation A only interacts with X within a cutoff distance of about 10 Å. When applying the BV model for Li pathway visualization, we calculate V(Li) for a hypothetical Li atom at a given position X, and assume $V_{\mathrm{ideal}}(\mathrm{Li}) = 1$. Then, the spatial function $|\Delta V(\mathrm{X})| = |V(\mathrm{Li}) - V_{\mathrm{ideal}}(\mathrm{Li})|$ can be used to visualize the Li charge density. The smaller this value, the larger should be the Li charge density. This BV method has been extensively used in searching for the Li path. For example, Adams *et al.*[22–26] developed a program based on the BV model to obtain the three-dimensional atomic valence map, which could be regarded as the "ion diffusion channel". They also related their BV calculated results to the energy manifold values (similar to the transition barrier).[25,26] Due to the low computational cost of this method, the group completed the calculation and screening of lithium ion diffusion channels in all alkaline earth metal ion materials in the Inorganic Crystal Structure Database (ICSD).[27] As another example, Chen *et al.*[28] combined the advantages of BV and DFT to perform high-throughput design and optimization of fast lithium ion conductors using β-Li_3PS_4.

However, the BV method only considers the Li interaction with anions, completely ignoring the existence and the position of cations. It is easy to imagine that this can lead to errors. Indeed, the diffusion pathways provided by the BV theory can often be different from those obtained by first-principles molecular dynamics simulations.[29,30] For example, in $LiFePO_4$, the BV pathway will include the Fe atom, while in Li_3N, the BV pathway is completely wrong. We will discuss these examples later in the paper.

Herein, we used the Ewald summation between the Li atom and the cathode atoms to overcome this shortcoming of the BV method. We only included the Li–cation interaction since the Li–anion interaction has already been taken into account by the BV method. We particularly calculated the Li-cation Coulomb interactions within a uniform negative charge background to compensate the total positive charge of the cations. To calculate such Coulomb interactions, the Ewald summation is used in both real space and reciprocal space.[31] The Ewald summation divides the long range Coulomb interaction into two parts: a short-range contribution, which is calculated in real space, and a long-range contribution, which is calculated using a Fourier transformation. By setting the G component in the Fourier space to be zero, the uniform negative charge background can be taken into account. Although the Ewald summation equation is very standard, we included it here for completeness:

$$U_{\mathrm{Ewald}} = U_{\mathrm{real}} + U_{\mathrm{reciprocal}} + U_{\mathrm{correction}} \tag{3}$$

where

$$U_{\mathrm{real}} = \frac{1}{4\pi\varepsilon_0}\frac{1}{2}\sum\nolimits_{\vec{n}}^{*}\sum_{i=1}^{N}\sum_{j=1}^{N} q_i q_j \frac{\mathrm{erfc}\left(\alpha\left|\vec{x}_{ij}+\vec{n}\right|\right)}{\left|\vec{x}_{ij}+\vec{n}\right|} \tag{4}$$

$$U_{\mathrm{reciprocal}} = \frac{1}{\varepsilon_0 V}\frac{1}{2}\sum_{\vec{k}\neq 0}\frac{1}{\vec{k}^2}\mathrm{e}^{-\frac{\vec{k}^2}{4\alpha}}\left[\left|\sum_{i=1}^{N} q_i \cos\left(\vec{k}\cdot\vec{x}\right)\right|^2 + \left|\sum_{i=1}^{N} q_i \sin\left(\vec{k}\cdot\vec{x}\right)\right|^2\right] \tag{5}$$

and $U_{\mathrm{correction}}$ is a constant depending on the parameter α. The converged results should not depend on the choice of α.

The Ewald Coulomb repulsive potentials (U_{Ewald}) were calculated on regular 3D real space grids for the Li position. In such a calculation, we assumed the test Li atoms walking through the whole 3D space. One issue is how to deal with the interaction of this test Li atom and the real Li atoms that exist in the crystal (*e.g.*, in its ground state position). Since we used this imaginary test Li atom to represent all the Li atoms in the

system, the repulsive interaction between this test Li atom to a nearby ground state Li atom was an erroneous interaction between the Li atom itself (since the test Li atom represented the nearby ground state Li atom with which it interacted). We thus needed to remove this "self-interaction". However, we should maintain the interactions with Li atoms that are far away since they are the "other" Li atoms. We thus have

$$U_e = U_{Ewald} - U_{Li} \quad (6)$$

and the following formula was used to calculate U_{Li} for interaction with nearby Li atoms:

$$U_{Li} = \frac{1}{4\pi\varepsilon_0}\sum_{R_{cut}}\frac{{q_{Li}}^2}{R}e^{-\beta\cdot R^2} \quad (7)$$

where R is the distance between the grid points (the position of the test Li atom) and the Li ions around that point and β is a parameter to control the range of this exclusion. We chose β equals one over square of 0.38 Å, which is half the lithium ion radius.

Now, we have two quantities: one is the BV valence V(Li) of eqn (2) and the other is the U_e of eqn (6). Our next task was to combine these two quantities into a single value to represent the Li concentration on the 3D grid. One option was to add them together as two energy components. Another option was to multiply them together as two factors. Adding them together required careful weighing in order to deal with their possible compensations. Tests showed that it was difficult to yield a reliable result. However, by multiplying them, we can require the system to satisfy two conditions: the bond valence to be close to 1, and U_e to be very negative (which is always negative due to the negative background compensation; thus, we require $|U_e|$ to be large). After some tests, we arrived at the following empirical expression:

$$E(\text{BV-Ewald}) = \frac{1}{|V(\text{Li}) - 1|^{10} + 1}|U_e| \quad (8)$$

The larger the value of E(BV-Ewald) is, the higher the probability of Li existing on the position. To visualize the Li path, we thus used an isosurface value E_{iso}. For a given position X in the real space 3D grid, if E(BV-Ewald) > E_{iso}, the lithium will occupy that point. This can thus give us the Li diffusion path. However, E_{iso} for different systems can be different. In practice, we can decrease the E_{iso} from large to small until the isosurface connects the Li path from one side of the crystal to the other side. In the following discussion, the Li path will be represented by the isosurface of E_{iso} plotted with the VESTA visualization package.[32] The computation time for most of the structure is several minutes, which improves the efficiency greatly compared with first-principles molecular dynamics simulation. Such a code can thus be used for high throughput screening of solid electrolyte materials. The BV code was written in python and the Ewald code was written in Fortran. The crystal structures were taken from the MP database[33] and Material Go database.[34]

3. Result and discussion

In order to test the accuracy of the BV-Ewald method, we predicted the diffusion pathways of several well-studied materials. The first material was $LiFePO_4$, which has attracted considerable interest and has already been used commercially as the cathode material for Li-ion batteries due to its environment-friendliness and the low cost of Fe element.[35] $LiFePO_4$ is an olivine-structured orthophosphate, as shown in Fig. 1. The left picture shows schematically the Li ion migration pathway calculated by *ab initio* molecular dynamics simulation.[33] The right picture shows the BV-Ewald result. The yellow part is the isosurface representing the Li clouds (populations) calculated by the BV-Ewald method with $E_{iso} = 42.5$. We can see that the Li ion migration pathway is along the b axis, which is in good agreement with the *ab initio* calculation results.[35,36]

It is helpful to understand the Li transition path in $LiFePO_4$ and why the BV-Ewald model can capture such transition pathways. There are three possible Li paths in $LiFePO_4$, as shown in Fig. 2. The path 1 along the b axis direction is clear from the PO_4 tetrahedron and the FeO_6 octahedron and there is no barrier when Li ion migrates along this path. However, in path 2 and 3, Li ion has to go through the side of PO_4 tetrahedron and FeO_6 octahedron, which influences the transfer of the Li ion. Furthermore, the distance from one Li ion location to another location along path 1 is the shortest (about 3.04 Å), compared with that along path 2 and path 3 (4.75 Å and 10.45 Å, respectively). Hence, the most possible Li migration pathway is path 1 along the b direction. Fisher *et al.*[35] calculated the Li ion migration energy of $LiFePO_4$. The energy barrier pathway of path 1 is 0.55 eV, the barrier of the path 2 is 2.89 eV and the barrier of the path 3 is 3.36 eV. Our BV-Ewald method calculates the Coulomb repulsive interaction between Fe/P and Li on every grid. The energy along path 1 is the smallest due to its relatively long distance from the cation. On the other hand, path 2 and 3 encounter the Fe/P cations in a short distance along the path, thus increasing their energies.

We have also performed calculations for several other well-known cathodes and solid electrolyte materials, namely, $LiMn_2O_4$, Li_3OCl, $LiM_2(PO_4)_3$ (M = Ti, Ge, Hf), α-Li_3N and β-Li_3N with their BV-Ewald Li diffusion paths shown in Fig. 3. These

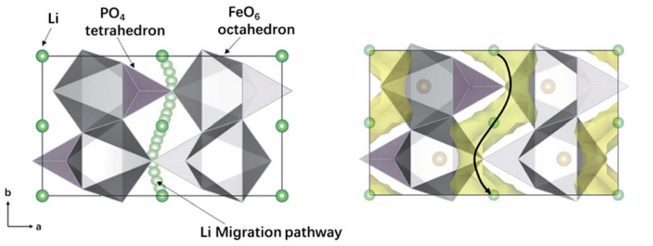

Fig. 1 Li migration pathway of $LiFePO_4$. (Left) Schematic view of the *ab initio* molecular simulation of the Li ion diffusion channel (ref. 26); (Right) BV-Ewald isosurface of the Li ion diffusion pathway with E_{iso} = 42.5. The black arrowed line in the right panel is a replot of the path from the left panel. The PO_4 tetrahedron is light purple and the silver-gray polyhedron is FeO_6 octahedron.

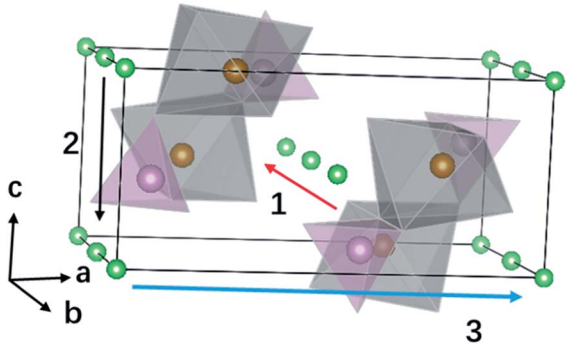

Fig. 2 Structure of $LiFePO_4$. The Li atom is green; the Fe atom is golden; the P atom is purple; the O atom is not shown.

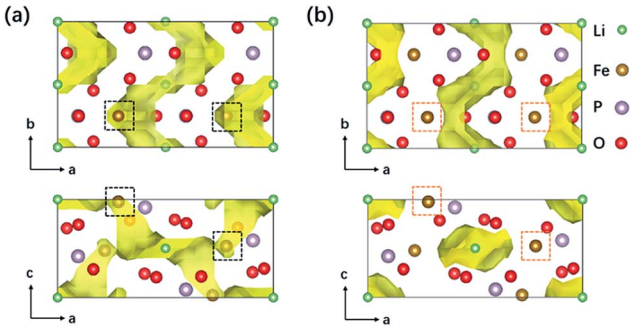

Fig. 4 (a) Li diffusion map of $LiFePO_4$ calculated by BV method; (b) Li diffusion map calculated by BV-Ewald method. The green ball is Li atom, the brownness ball is Fe atom, the light purple ball is phosphorus atom and the red ball is oxygen atom.

systems were selected due to the existence of *ab initio* molecular dynamics (MD) simulations of their Li diffusion paths. The results of these *ab initio* MD simulations are summarized for their Li diffusion paths, as represented by the arrow lines in Fig. 3. As can be seen in Fig. 3, the BV-Ewald reproduced these *ab initio* paths perfectly. This demonstrates a major success for the BV-Ewald method.

In the following discussion, we compare the BV-Ewald results with the BV result to see the cases where the BV-Ewald is an improvement over the BV result. We again used $LiFePO_4$ as our first example. As illustrated in Fig. 4, the left part (a) is the Li ion diffusion map calculated by the BV method (with isosurface on $|V(\mathrm{Li}) - 1| < 0.1$) and the right part (b) is the BV-Ewald calculated result. We find that both methods show the Li migration pathway along the *b* axis. However, there is a crucial difference. As circled in the black square in Fig. 4a, the BV Li map includes Fe atoms inside its isosurface regardless of the chosen isosurface value. This is clearly not correct since it implies that Li will be in the position of the Fe atoms. This result is obtained on ignoring the Li-cation repulsion. On the contrary, the BV-Ewald Li map does not contain the Fe atom, as shown in Fig. 4b.

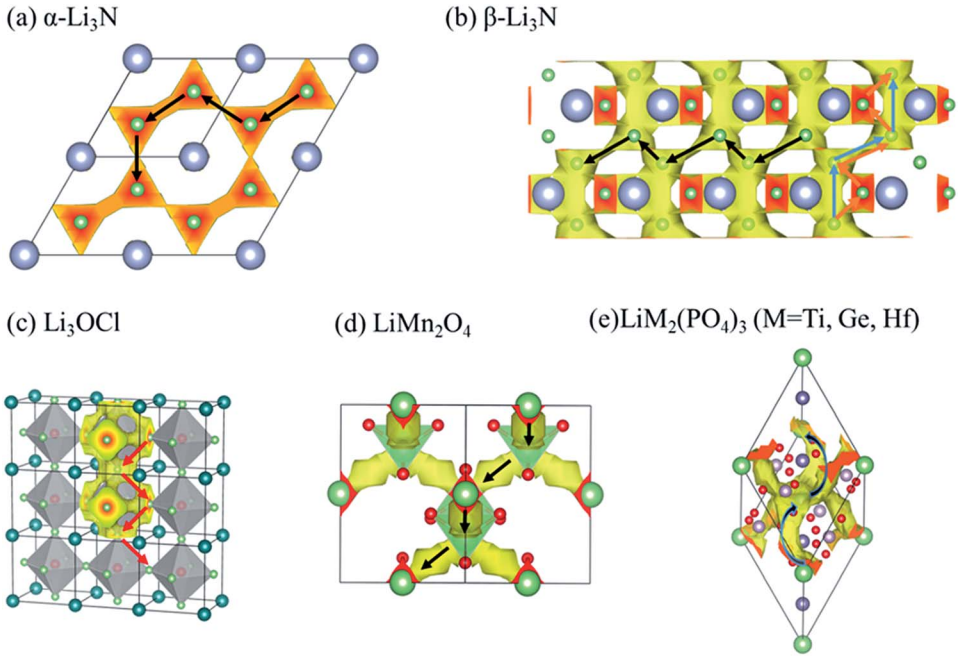

Fig. 3 Comparison between ab initial path (arrowed lines) and BV-Ewald path (yellow isosurface) of Li diffusion pathways: (a) Li migration pathway of α-Li_3N. First-principles calculations of Li ion diffusion channel[9] and BV-Ewald result of Li ion diffusion pathway when $E_{iso} = 3.6$. (b) Li migration pathway of β-Li_3N. First-principles calculations of Li ion diffusion channel[9] and BV-Ewald result of Li ion diffusion pathway when $E_{iso} = 6$. (c) Li migration pathway of Li_3OCl. The arrow shows the migration pathway calculated by *ab initio* calculations and the Gibbs energy down the route goes from *ca.* 0.290 eV at 0 K to *ca.* 0.245 eV before the melting point (550 K)[37] and the yellow part is BV-Ewald result of Li ion diffusion pathway when $E_{iso} = 2.6$. (d) Li migration pathway of $LiMn_2O_4$. First-principles calculations of the Li ion diffusion channel[38] and the BV-Ewald result of Li ion diffusion pathway when $E_{iso} = 70$. (e) Li migration pathway of $LiM_2(PO_4)_3$ (M = Ti, Ge, Hf).[39] Negative nuclear density maps after MEM reconstruction and the BV-Ewald result of Li ion diffusion pathway when $E_{iso} = 139.5$.

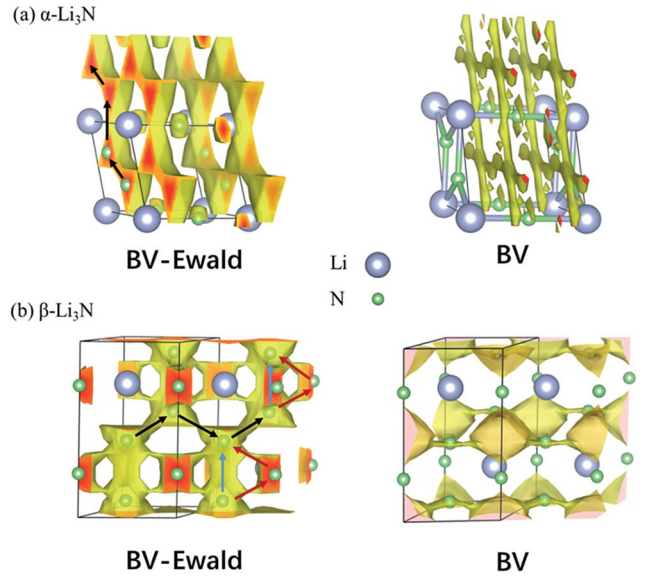

Fig. 5 (a) Li diffusion map of α-Li_3N; (b) Li diffusion map of β-Li_3N. The green ball is Li and grey ball is N. The arrows describe the Li ion migration pathway by using first-principles calculations.

In the above example of $LiFePO_4$, although the isosurface between BV and BV-Ewald are different around the Fe position, their Li diffusion paths are roughly the same. However, this is not always the case for other systems. We find that the BV and BV-Ewald Li ion diffusion pathways for Li_3N are completely different. In Fig. 5, the left picture is the result of the BV-Ewald method and the right picture is the result of BV theory. The arrows describe the Li ion migration pathway based on first-principles calculations.[9] We can see that the BV-Ewald results of α-Li_3N and β-Li_3N are in good agreement with the observed pathway, but the BV results are completely different. In α-Li_3N, the Li ion is more likely to migrate a shorter distance in the plane comprising both N and Li. In β-Li_3N, Li migration pathways also prefer the shorter Li hopping distance channel and there are three possible pathways because their hopping distances are similar. The main difference between the BV and BV-Ewald methods is for the Li–Li interaction. For example, for the α-Li_3N, in the BV method, the pathways are in the plane of the pure Li atoms. On the other hand, due to Li–Li repulsion, in the BV-Ewald method, the pathways have been pushed into the Li–N plane, which agrees with the first-principles results. This example shows that the Li–cation interaction as included in the BV-Ewald method can play an important role in determining the true Li diffusion path in the material. Thus, the BV-Ewald method can be used for high throughput identification of the Li-pathway in different types of cathode and solid-electrolyte materials.

Taking advantage of the fast calculation speed, we performed calculations for 34 typical solid state electrolytes and electrode materials. Although all these materials are known, not all their Li diffusion paths have been studied theoretically. We aimed at identifying the dimensionality of their Li diffusion path. This is defined as the connection dimension for the highest isosurface value where at least one direction has been connected. If only one direction has been connected at this isosurface value, the system will be called 1D. In some systems, due to symmetry or other reasons, at this isosurface value or a slightly larger value (+0.5), two directions or all three directions will be connected, resulting in their dimensionality being 2D or 3D, respectively. For example, the 1D pathway along the *b* direction in $LiFePO_4$ initially appears with decreasing isosurface values, so its pathway is 1D. On the other hand, for $LiMn_2O_4$, 3 equivalent paths along three directions are all connected for a given isosurface value, so its dimensionality is 3D. Tables 1 and 2 show the crystallographic details and proposed dimensionality for the Li ion diffusion pathway for electrode materials and electrolyte materials respectively. The Li diffusion isosurfaces of these 34 crystals are all shown in Fig. S1.†

Finally, it should be noted that in this study, we mainly focused on the visualization of the Li ion diffusion path. An equally important task was to estimate the diffusion barrier height. It turns out that this is a much more challenging task. In order to yield accurate barrier heights, real energy estimation instead of merit functions such as eqn (8) need to be used. Tests show that it is difficult to use eqn (8) to estimate the barrier height. Such a task needs to be worked on in the future.

4. Conclusions

In this paper, we presented a new high throughput method for identifying the Li-diffusion pathways for the Li-ion cathode and solid-electrolyte materials by combining BV theory with the Ewald summation between Li and the cation. This method improves over the original BV model by including information for the Li-cation repulsion. We first calculated several common

Table 1 Crystallographic details and proposed dimensionality of Li ion migration pathway for electrode materials

Electrode materials								
Compound	Space group	*a* (Å)	*b* (Å)	*c* (Å)	*α* (°)	*β* (°)	*γ* (°)	Dimensionality
$LiFePO_4$	*Pnma*	10.45067	6.08735	4.75196	90	90	90	1D
$LiCoO_2$	$R\bar{3}m$	2.8156	2.8156	14.0542	90	90	120	2D
Li_2TiO_3	*C*2/*c*	5.0996	8.85271	9.83459	90	100.2	90	3D
$LiMn_2O_4$	$Fd\bar{3}m$	8.4307	8.4307	8.4307	90	90	90	3D
$LiMnO_2$	*Pmmn*	2.86878	4.63448	5.83251	90	90	90	2D

Table 2 Crystallographic details and proposed dimensionality of Li ion migration pathway for solid-state electrolytes

Compound	Space group	a (Å)	b (Å)	c (Å)	α (°)	β (°)	γ (°)	Dimensionality
(Anti)perovskite								
Li_3OCl	$Pm\bar{3}m$	3.90834	3.90834	3.90834	90	90	90	3D
Li_2OHCl	$Pm4m$	3.91	3.91	3.91	90	90	90	2D
$LiLa_5Ti_8O_{24}$	$Pmm2$	7.85238	7.82107	7.7691	90	90	90	2D
NASICON								
$LiTi_2(PO_4)_3$	$R\bar{3}c$	8.61194	8.61194	8.61994	60	60	60	3D
$LiGe_2(PO_4)_3$	$R\bar{3}c$	8.4397	8.4397	8.4397	60	60	60	3D
$LiHf_2(PO_4)_3$	$R\bar{3}c$	8.83	8.83	8.83	60	60	60	3D
LISICON								
β-Li_3PS_4	$Pnma$	13.18362	8.13245	6.21318	90	90	90	3D
$Li_{10}GeP_2S_{12}$	$P4_2mc$	8.78765	8.78765	12.65755	90	90	90	3D
$Li_{10}SiP_2S_{12}$	$P4_2mc$	8.78389	8.78389	12.60642	90	90	90	3D
$Li_{10}SnP_2S_{12}$	$P4_2mc$	8.85424	8.85424	12.85128	90	90	90	3D
Garnet								
$Li_7La_3Zr_2O_{12}$	$I4_1/acd$	13.23937	13.23937	12.76846	90	90	90	3D
$Li_5La_3Nb_2O_{12}$	$Ia\bar{3}d$	11.36758	11.36758	11.36758	109.47	109.47	109.47	3D
$Li_5La_3Ta_2O_{12}$	$Ia\bar{4}d$	11.35147	11.35147	11.35147	109.47	109.47	109.47	3D
Li-nitride								
α-Li_3N	$P6/mmm$	3.65069	3.65069	3.88863	90	90	120	2D
β-Li_3N	$P6_3/mmc$	3.56452	3.56452	6.34898	90	90	120	2D
Li_7PN_4	$P4\bar{3}n$	9.40238	9.40238	9.40238	90	90	90	3D
$LiPN_2$	$I\bar{4}d$	4.57145	4.57145	7.28985	90	90	90	3D
$LISi_2N_3$	$Cmc2_1$	4.8144	5.33094	5.33094	119.88	90	90	1D
Li-hydride								
Li_2HN	$R3m$	3.6031	3.6031	9.09702	90	90	90	2D
LiH_2N	$I\bar{4}$	5.067	5.067	10.284	90	90	90	3D
$LiBH_4$	$P6_3mc$	4.17997	4.17997	6.71	90	90	120	2D
Li_3AlH_6	$R\bar{3}$	4.53	9.27	2.86	90	90	90	3D
$LIAlH_4$	$I4_1/a$	4.5776	4.5776	10.16941	90	90	90	2D
Li-halide								
Li_2CdCl_4	$Imma$	7.58329	7.76592	10.59649	90	90	90	3D
Li_2MgCl_4	$Imma$	7.4119	7.48861	10.48336	90	90	90	3D
Li_2ZnI_4	$Pnma$	7.06393	8.68383	15.00896	90	90	90	2D
Argyrodite								
Li_6PS_5Br	$F4\bar{3}m$	10.305	10.305	10.305	90	90	90	3D
Li_6PS_5Cl	$F4\bar{3}m$	10.279	10.279	10.279	90	90	90	3D
Li_6PS_5I	$F4\bar{3}m$	10.353	10.353	10.353	90	90	90	3D

solid state electrolytes and electrode materials, namely, $LiFePO_4$ and Li_3N, and compared their Li ion diffusion pathways with those obtained by first-principles results in the literature. We found that the improved BV-Ewald model yields Li diffusion pathways that are in excellent agreement with those obtained by *ab initio* results. In contrast, the original BV model might yield the wrong path or indicate Li clouds on top of other cathode atoms. We also performed calculations for 34 different known electrodes and electrolytes. We provided their Li path dimensionalities as well as the detailed Li path isosurfaces, which have not been studied before theoretically. The BV-Ewald model is fast to calculate, and we believe the new BV-Ewald model can be used for future high throughput simulations for new solid electrolyte discovery. This model can also be used for initial screening prior to in-depth *ab initio* simulations for a given material.

Conflicts of interest

There are no conflicts to declare.

Acknowledgements

Wang's research is supported by the Assistant Secretary for Energy Efficiency and Renewal Energy of the U.S. Department of Energy under the Battery Materials Research (BMR) program. This study was also financially supported by National Key R&D Program of China (2016YFB0700600), and Shenzhen Science

and Technology Research Grant (No. JCYJ20150729111733470 and No. JCYJ20151015162256516).

References

1 J. M. Tarascon and M. Armand, *Mater. Sustainable Energy*, 2010, **414**, 171–179.
2 E. Karden, S. Ploumen, B. Fricke, T. Miller and K. Snyder, *J. Power Sources*, 2007, **168**, 2–11.
3 J. B. Goodenough and Y. Kim, *Chem. Mater.*, 2010, **22**, 587–603.
4 K. Xu, *Chem. Rev.*, 2004, **104**, 4303–4418.
5 K. Takada, *Acta Mater.*, 2013, **61**, 759–770.
6 M. Yashima, M. Itoh, Y. Inaguma and Y. Morii, *J. Am. Chem. Soc.*, 2005, **127**, 3491–3495.
7 J. Han, J. Zhu, Y. Li, X. Yu, S. Wang, G. Wu, H. Xie, S. C. Vogel, F. Izumi, K. Momma, Y. Kawamura, Y. Huang, J. B. Goodenough and Y. Zhao, *Chem. Commun.*, 2012, **48**, 9840.
8 C. A. Geiger, E. Alekseev, B. Lazic, M. Fisch, T. Armbruster, R. Langner, M. Fechtelkord, N. Kim, T. Pettke and W. Weppner, *Inorg. Chem.*, 2011, **50**, 1089–1097.
9 W. Li, G. Wu, C. M. Araújo, R. H. Scheicher, A. Blomqvist, R. Ahuja, Z. Xiong, Y. Feng and P. Chen, *Energy Environ. Sci.*, 2010, **3**, 1524.
10 S. Adams and R. P. Rao, *J. Mater. Chem.*, 2012, **22**, 1426–1434.
11 S. Adams and R. Prasada Rao, *J. Mater. Chem.*, 2012, **22**, 7687.
12 S. Adams, *Solid State Ionics*, 2002, **154–155**, 151–159.
13 S. Adams, *J. Power Sources*, 2006, **159**, 200–204.
14 V. Thangadurai, S. Adams and W. Weppner, *Chem. Mater.*, 2004, **16**, 2998–3006.
15 N. A. Anurova and V. A. Blatov, *Acta Crystallogr., Sect. B: Struct. Sci.*, 2009, **65**, 426–434.
16 G. Nuspl, T. Takeuchi, A. Weiß, H. Kageyama, K. Yoshizawa and T. Yamabe, *J. Appl. Phys.*, 1999, **86**, 5484–5491.
17 M. Ø. Filsø, M. J. Turner, G. V. Gibbs, S. Adams, M. A. Spackman and B. B. Iversen, *Chem.–Eur. J.*, 2013, **19**, 15535–15544.
18 I. D. Brown, *Chem. Rev.*, 2009, **109**, 6858–6919.
19 X. Zhao, X. Zhang, D. Wu, H. Zhang, F. Ding and Z. Zhou, *J. Mater. Chem. A*, 2016, **4**, 16606–16611.
20 X. Zhang, Z. Zhang, S. Yao, A. Chen, X. Zhao and Z. Zhou, *npj Comput. Mater.*, 2018, **4**, 13–18.
21 Y. Zhu, X. He and Y. Mo, *J. Mater. Chem. A*, 2016, **4**, 3253–3266.
22 S. Adams, *Acta Crystallogr., Sect. B: Struct. Sci.*, 2001, **57**, 278–287.
23 S. Adams and J. Swenson, *Phys. Rev. Lett.*, 2000, **84**, 4144–4147.
24 S. Adams and R. P. Rao, in *Bond Valences*, ed. I. D. Brown and K. R. Poeppelmeier, Springer Berlin Heidelberg, Berlin, Heidelberg, 2014, vol. 158, pp. 129–159.
25 S. Adams and R. P. Rao, *Phys. Status Solidi A*, 2011, **208**, 1746–1753.
26 S. Adams and R. Prasada Rao, *Phys. Chem. Chem. Phys.*, 2009, **11**, 3010.
27 M. Avdeev, M. Sale, S. Adams and R. P. Rao, *Solid State Ionics*, 2012, **225**, 43–46.
28 R. Xiao, H. Li and L. Chen, *Sci. Rep.*, 2015, **5**, 1–11.
29 G. Kresse and J. Hafner, *Phys. Rev. B: Condens. Matter Mater. Phys.*, 1996, **47**, 558–561.
30 G. Kresse and J. Furthmüller, *Phys. Rev. B: Condens. Matter Mater. Phys.*, 1996, **54**, 11169–11186.
31 T. Matthey, https://core.ac.uk/display/20697861, 2005.
32 K. Momma and F. Izumi, *J. Appl. Crystallogr.*, 2008, **41**, 653–658.
33 A. Jain, S. P. Ong, G. Hautier, W. Chen, W. D. Richards, S. Dacek, S. Cholia, D. Gunter, D. Skinner, G. Ceder and K. A. Persson, *APL Mater.*, 2013, **1**, 011002.
34 pkusam, http://www.pkusam.com/, accessed August 12, 2018.
35 C. A. J. Fisher, V. M. Hart Prieto and M. S. Islam, *Chem. Mater.*, 2008, **20**, 5907–5915.
36 J. Yang and J. S. Tse, *J. Phys. Chem. A*, 2011, **115**, 13045–13049.
37 R. Mouta, M. Á. B. Melo, E. M. Diniz and C. W. A. Paschoal, *Chem. Mater.*, 2014, **26**, 7137–7144.
38 N. Ishizawa, D. du Boulay, M. Hayatsu, S. Kuze, Y. Matsushima, H. Ikuta, M. Wakihara, Y. Tabira and J. R. Hester, *J. Solid State Chem.*, 2003, **174**, 167–174.
39 M. Monchak, T. Hupfer, A. Senyshyn, H. Boysen, D. Chernyshov, T. Hansen, K. G. Schell, E. C. Bucharsky, M. J. Hoffmann and H. Ehrenberg, *Inorg. Chem.*, 2016, **55**, 2941–2945.

